

Quantum structural fluctuation in para -hydrogen clusters revealed by the variational path integral method

メタデータ	言語: eng 出版者: 公開日: 2018-04-05 キーワード (Ja): キーワード (En): 作成者: メールアドレス: 所属:
URL	https://doi.org/10.24517/00050467

This work is licensed under a Creative Commons Attribution-NonCommercial-ShareAlike 3.0 International License.



Quantum structural fluctuation in para-hydrogen clusters revealed by the variational path integral method

Shinichi Miura

Citation: *The Journal of Chemical Physics* **148**, 102333 (2018);

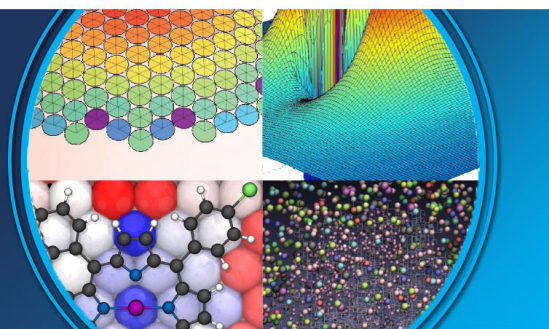
View online: <https://doi.org/10.1063/1.5005126>

View Table of Contents: <http://aip.scitation.org/toc/jcp/148/10>

Published by the [American Institute of Physics](#)

AIP | The Journal of
Chemical Physics

PERSPECTIVES



Quantum structural fluctuation in *para*-hydrogen clusters revealed by the variational path integral method

Shinichi Miura^{a)}

Faculty of Mathematics and Physics, Kanazawa University, Kakuma, Kanazawa 920-1192, Japan

(Received 17 September 2017; accepted 18 December 2017; published online 8 January 2018)

In this paper, the ground state of *para*-hydrogen clusters for size regime $N \leq 40$ has been studied by our variational path integral molecular dynamics method. Long molecular dynamics calculations have been performed to accurately evaluate ground state properties. The chemical potential of the hydrogen molecule is found to have a zigzag size dependence, indicating the magic number stability for the clusters of the size $N = 13, 26, 29, 34,$ and 39 . One-body density of the hydrogen molecule is demonstrated to have a structured profile, not a melted one. The observed magic number stability is examined using the inherent structure analysis. We also have developed a novel method combining our variational path integral hybrid Monte Carlo method with the replica exchange technique. We introduce replicas of the original system bridging from the structured to the melted cluster, which is realized by scaling the potential energy of the system. Using the enhanced sampling method, the clusters are demonstrated to have the structured density profile in the ground state. *Published by AIP Publishing.* <https://doi.org/10.1063/1.5005126>

I. INTRODUCTION

Molecular *para*-hydrogen has been suggested to be a possible natural superfluid other than liquid ^4He .¹ However, attractive interaction between hydrogen molecules is so strong, which is about three times larger than helium-helium attraction, that liquid *para*-hydrogen crystallizes before arriving at the superfluid transition temperature; the triple point of hydrogen is located at 13.96 K. Ginzburg and Sobayanin¹ have pointed out that the condensed hydrogen could undergo the superfluid transition in the supercooled state; they roughly estimated the transition temperature to be about 6 K using the ideal Bose gas theory. The more elaborate estimation of the superfluid transition using the path integral Monte Carlo (PIMC) method² is found to be the transition temperature about 1 K. Many attempts to supercool liquid hydrogen down to the expected lambda transition have been unfruitful for the bulk phases. Partial success has been achieved in confined geometries, mainly in small isolated clusters³ or larger clusters in a ^4He nanodroplet.^{4,5}

Para-hydrogen clusters have been studied by quantum simulation methods in the last few decades.^{6–21} The first path integral Monte Carlo (PIMC) study⁶ showed that the *para*-hydrogen clusters of sizes $N = 13$ and 18 are superfluid at temperatures below 2 K. Then, properties including superfluidity of clusters $N \leq 40$ have systematically been studied by the PIMC method;¹¹ clusters with $N < 26$ have significant superfluid fraction at $T \leq 1.5$ K. For larger clusters, superfluidity is quenched for magic number clusters revealed by energetic analysis. They¹¹ found that the superfluidity is localized at the surface of the cluster. This localized

superfluidity has been questioned in another PIMC study¹⁴ where it has been shown that the superfluidity is a global property of the cluster in spite of its significant spatial structure. They¹⁴ also suggested that with further lowering temperature, a liquid-like structure emerges; the cluster undergoes “quantum melting.”

In the limit of zero temperature, the structure and energy of *para*-hydrogen clusters have been studied using diffusion Monte Carlo (DMC)^{9,15} and path integral ground state (PIGS).^{8,16,20} The stability of the clusters was examined by the chemical potential of the hydrogen molecule. DMC chemical potential showed monotonic size dependence for $N > 20$; on the other hand, the PIMC counterpart¹¹ in the same size regime showed a zigzag size dependence indicating the magic number stability mentioned above. Although PIGS chemical potential agrees well with DMC results up to $N = 33$, magic number stability was found for larger clusters. On the other hand, PIGS results reported in Ref. 16 are in disagreement with PIMC results,¹¹ missing some magic number clusters found in the PIMC study.

In the present study, two issues on the *para*-hydrogen clusters have been addressed. One is the size dependence of the chemical potential; even for the ground states, a consensus has not yet been reached as described above. The other is the structure of the clusters. While the PIMC calculations¹⁴ have suggested that the clusters have a liquid-like melted structure around the temperature down to 0.06 K, which is demonstrated for $N = 26$, the ground state quantum Monte Carlo (QMC) calculations have indicated that the clusters have the shell structure.

In this paper, we systematically study the size dependence of the cluster stability up to the size of $N \leq 40$ by the variational path integral (VPI) method. The variational path integral,²² which is also called the path integral ground state,²³

^{a)}Electronic mail: smiura@mail.kanazawa-u.ac.jp

is a method to numerically solve many-body ground states exactly. Our molecular dynamics (MD) method of the variational path integral referred as the variational path integral molecular dynamics (VPIMD)^{24–32} is applied to explore the ground state of the *para*-hydrogen clusters. Our preliminary studies on the *para*-hydrogen clusters for $N \leq 20$ using VPIMD are found in Refs. 28 and 29. In this study, the size regime is extended up to $N = 40$; much longer molecular dynamics calculations than the previous studies have been performed to accurately evaluate the total energy and associated chemical potential. We also have developed a novel method to efficiently sample the ground state of many-body systems, combining our variational path integral hybrid Monte Carlo (VPIHMC),^{30,32} which is an equation-of-motion guided Monte Carlo (MC), with the replica exchange technique.^{33,34} Using replicas of the original system by scaling the potential energy of the cluster, we can sample the configuration space much wider than the standard method; possible sampling problems arising from trapping of the system in a metastable state can be excluded using the replicas connecting the original system with a fictitious liquid-like melted structure.

This paper is organized as follows. We present our method regarding the variational path integral in Sec. II. Computational details are given in Sec. III. Systematic size dependence of energy and structure and associated inherent structure analysis of the ground state *para*-hydrogen clusters are presented in Secs. IV and V, respectively. In Sec. VI, the replica exchange VPIHMC results are presented for selected clusters, $N = 25$, 26, and 27. Concluding remarks are given in Sec. VII.

II. METHODOLOGY

A. The variational path integral method

In this section, we briefly summarize the variational path integral (VPI) method.²² We begin to consider a system consisting of N particles governed by a Hamiltonian $\hat{H} = \hat{T} + \hat{V}$, where \hat{T} and \hat{V} are kinetic and potential energy operators, respectively. Using a trial wavefunction of a target system $|\Phi_T\rangle$, the exact ground state $|\Psi_0\rangle$ can be obtained by the following relation:^{22,35}

$$|\Psi_0\rangle = \lim_{\beta \rightarrow \infty} e^{-(\beta/2)\hat{H}} |\Phi_T\rangle, \quad (1)$$

where β is a real parameter called a projection time or an imaginary time. This relation indicates that the exact ground state wavefunction can be extracted from the trial wavefunction if β is long enough. Here, we consider a scalar product of the ground state referred to be a pseudo partition function, which plays a central role to construct the VPI expressions,²²

$$\begin{aligned} Z_0 &= \langle \Psi_0 | \Psi_0 \rangle = \langle \Phi_T | e^{-\beta \hat{H}} | \Phi_T \rangle \\ &= \int \int dR dR' \langle \Phi_T | R \rangle \langle R | e^{-\beta \hat{H}} | R' \rangle \langle R' | \Phi_T \rangle, \end{aligned} \quad (2)$$

where the coordinates of N particles are represented collectively to be $R = (r_1, \dots, r_N)$ and we have used the closure relation regarding coordinate basis $\int dR |R\rangle \langle R| = 1$. A matrix element $\langle R | e^{-\beta \hat{H}} | R' \rangle$ in Eq. (2) is the density matrix at the inverse temperature β , $\rho(\beta, R, R')$.^{36,37} The density matrix

can be written on the basis of the discretized path integral by^{22,38,39}

$$\rho(R, R'; \beta) \propto \int dR^{(1)} \dots \int dR^{(M-1)} e^{-S(R; \Delta\tau)/\hbar}, \quad (3)$$

where S and $\Delta\tau = \beta/M$ are the discretized imaginary time action and the associated imaginary time increment, respectively; coordinates at all the imaginary time slices are collectively denoted by $\{R\} = (R^{(0)}, \dots, R^{(s)}, \dots, R^{(M)})$. The explicit expression of the action S depends on the approximation scheme adopted. In this study, the following Suzuki-Chin type fourth order formula^{40–43} is adopted:

$$e^{-2\Delta\tau\hat{H}} = e^{-\frac{\Delta\tau}{3}\hat{V}_e} e^{-\Delta\tau\hat{T}} e^{-\frac{4}{3}\Delta\tau\hat{V}_m} e^{-\Delta\tau\hat{T}} e^{-\frac{\Delta\tau}{3}\hat{V}_e} + \mathcal{O}(\Delta\tau^5), \quad (4)$$

where γ is an arbitrary constant in the range of $[0,1]$ and

$$\begin{aligned} V_e &= V + \frac{\gamma}{6}\Delta\tau^2 [V, [T, V]], \\ V_m &= V + \frac{1-\gamma}{12}\Delta\tau^2 [V, [T, V]]. \end{aligned} \quad (5)$$

The commutator above can be written by

$$[V, [T, V]] = \sum_{i=1}^N \frac{\hbar^2}{m_i} \left(\frac{\partial V}{\partial r_i} \right)^2, \quad (6)$$

where m_i is the atomic mass of an i th particle. Then, the pseudo partition function can be written as

$$Z_0 \propto \int dR^{(0)} \dots \int dR^{(M)} \Phi_T(R^{(0)}) e^{-S(R; \Delta\tau)/\hbar} \Phi_T(R^{(M)}). \quad (7)$$

Various physical quantities can be evaluated on the basis of the above expression. The ground state energy is evaluated by³⁵

$$E_0 = \frac{\langle \Psi_0 | \hat{H} | \Psi_0 \rangle}{\langle \Psi_0 | \Psi_0 \rangle} = \frac{\langle \Phi_T | \hat{H} e^{-\beta \hat{H}} | \Phi_T \rangle}{Z_0}, \quad (8)$$

where we have used Eq. (1) and the commutability of \hat{H} and $e^{-\beta \hat{H}}$. In the vanishing projection time limit, the right-hand side of Eq. (8) gives the variational energy by the trial wavefunction we adopt. We can automatically improve the variational estimate of the ground state energy by increasing β ; then, the exact ground state energy is obtained using a sufficiently long projection time. Probability density by the exact wavefunction, $\rho(R)$, is given by

$$\rho(R) = \frac{\langle \Psi_0 | \delta(\hat{R} - R) | \Psi_0 \rangle}{Z_0} = \frac{|\Psi_0(R)|^2}{Z_0}. \quad (9)$$

This quantity is given using Eq. (1) to be the probability density of the system at the imaginary time $\tau = \beta/2$,

$$\rho(R) = \frac{\langle \Phi_T | e^{-(\beta/2)\hat{H}} \delta(\hat{R} - R) e^{-(\beta/2)\hat{H}} | \Phi_T \rangle}{Z_0}. \quad (10)$$

This indicates that the expected value of physical quantities diagonal in the coordinate space is exactly evaluated by the variational path integral.

B. Molecular dynamics and hybrid Monte Carlo algorithms

As in the standard path integral method for finite temperature systems,^{22,38,39} the pseudo partition function Z_0 , Eq. (7),

can be regarded as a configuration integral of classical polymers. In the variational path integral, the classical isomorphic systems consist of open chain polymers. Furthermore, distributions of end-point coordinates of the polymers are affected by the trial wavefunction $\Phi_T(R^{(0)})$ and $\Phi_T(R^{(M)})$, respectively. Here, we define the following effective interaction for the polymeric systems W_{eff} :

$$W_{\text{eff}}(\{R\}) = \frac{S(\{R\})}{\beta} - \frac{\ln \Phi_T(R^{(0)})}{\beta} - \frac{\ln \Phi_T(R^{(M)})}{\beta}, \quad (11)$$

with

$$\frac{1}{\beta} S(\{R\}) = \sum_{s=0}^{M-1} \sum_{i=1}^N \frac{1}{2} m_i \omega_M^2 (r_i^{(s)} - r_i^{(s+1)})^2 + \frac{1}{M} \sum_{s=0}^M \bar{V}(R^{(s)}), \quad (12)$$

where $\omega_M = \sqrt{M}/\beta\hbar$ and $\bar{V}(R)$ is the intermolecular interaction including the fourth order correction whose explicit expression is found elsewhere.^{30,32} Then, the pseudo partition function Eq. (7) is rewritten by

$$Z_0 \propto \int dR^{(0)} \dots \int dR^{(M)} e^{-\beta W_{\text{eff}}(\{R\})}. \quad (13)$$

The above integral can be interpreted to be a canonical partition function for the classical polymers with the interaction W_{eff} . Then, molecular simulation techniques designed to generate the canonical ensemble can be used to perform the VPI calculations. We first describe the molecular dynamics algorithm.²⁴ We define the following classical Hamiltonian:

$$H_{\text{VPIMD}} = \sum_{s=0}^M \sum_{i=1}^N \frac{p_i^{(s)2}}{2m_i^{(s)}} + W_{\text{eff}}(\{R\}), \quad (14)$$

where $p_i^{(s)}$ denotes the fictitious momentum of an i th particle at an s th time slice and $m_i^{(s)}$ is the associated fictitious mass. Using the above Hamiltonian, we can derive the equations of motion based on the Hamilton's canonical equation. Then, in order to generate the canonical ensemble, we attach a single Nosé-Hoover chain thermostat⁴⁴ to each degree of freedom.^{45,46} The resulting equations of motion are basic equations for the variational path integral molecular dynamics (VPIMD) method. Usually, generalized coordinates diagonalizing harmonic interactions in Eq. (12) such as normal mode and staging coordinates are adopted for efficient calculations.³⁹

The hybrid Monte Carlo (HMC)^{45,47,48} is another method to generate the canonical ensemble, which is an equation-of-motion guided Monte Carlo method. Unlike the standard MC, whole system coordinates are simultaneously updated by equations of motion. The trial configuration is then accepted or rejected by an appropriate Metropolis criterion as in MC. To construct the HMC method for the variational path integral, the above Hamiltonian H_{VPIMD} is used to introduce the equations

of motion. The variational path integral hybrid Monte Carlo (VPIHMC) method^{30,32} is outlined as follows. We start with an initial state of the system ($\{P\}$, $\{R\}$) and resample momenta $\{P\}$ from the Maxwell distribution. Here, $\{P\}$ collectively denotes fictitious momenta of particles at all the imaginary time slices. Molecular dynamics is used to move the whole system for time increment of $n_{\text{MD}} \times \Delta t$, where Δt is the time increment of the MD calculation and n_{MD} is the number of MD step in one HMC cycle. The trial configuration is then accepted by the probability P_A ,

$$P_A = \min\{1, e^{-\beta \Delta H_{\text{VPIMD}}}\}, \quad (15)$$

where ΔH_{VPIMD} is the change in the total Hamiltonian H_{VPIMD} after the move of n_{MD} steps. When we adopt the fourth order approximation, the effective interaction among the polymers includes the square of the gradient of the potential function. The Hessian matrix of the potential has to be calculated to evaluate the force in MD and the above HMC. We can avoid the evaluation of the Hessian matrix by introducing a multilevel description in the HMC trial move. A detailed description on the multilevel HMC method can be found elsewhere.^{30,32}

C. Replica exchange extension

Here, we consider extending our hybrid Monte Carlo method to combine the idea of the replica exchange Monte Carlo.^{33,34} We first prepare L replicas of the system considered. Each replica is the same as the original system except the intermolecular interaction; an intermolecular interaction for an ℓ th replica is given to be the original interaction scaled by a constant less than unity $\alpha^{[\ell]}$, $\alpha^{[\ell]}V$. The associated effective interaction is expressed to be $W_{\text{eff}}^{[\ell]}(\{R\}^{[\ell]})$ where the coordinates of the ℓ th replica are denoted by $\{R\}^{[\ell]}$. In the replica exchange method, we consider an extended configuration space X ,

$$X = (\{R\}^{[1]}, \dots, \{R\}^{[\ell]}, \dots, \{R\}^{[L]}). \quad (16)$$

The probability density in the extended configuration space $P_{\text{ex}}(X)$ is defined by

$$P_{\text{ex}}(X) = \prod_{\ell=1}^L P(\{R\}^{[\ell]}). \quad (17)$$

Each replica obeys the canonical density $P(\{R\}^{[\ell]})$,

$$P(\{R\}^{[\ell]}) = \frac{e^{-\beta W_{\text{eff}}^{[\ell]}(\{R\}^{[\ell]})}}{Z_0^{[\ell]}}, \quad (18)$$

where $Z_0^{[\ell]}$ is the pseudo partition function for the ℓ th replica.

We next consider a trial move to exchange configurations of an m th replica $\{R\}$ with those of an n th replica $\{R'\}$. The detailed balance condition for the move is given by

$$\begin{aligned} P_{\text{ex}}(\dots; \{R\}, W_{\text{eff}}^{[m]}; \dots; \{R'\}, W_{\text{eff}}^{[n]}; \dots) T(\{R\}, W_{\text{eff}}^{[m]} | \{R'\}, W_{\text{eff}}^{[n]}) &= P_{\text{ex}}(\dots; \{R'\}, W_{\text{eff}}^{[m]}; \dots; \{R\}, W_{\text{eff}}^{[n]}; \dots) \\ &\times T(\{R'\}, W_{\text{eff}}^{[n]} | \{R\}, W_{\text{eff}}^{[m]}), \end{aligned} \quad (19)$$

where $T(\{R\}, W_{\text{eff}}^{[m]}|\{R'\}, W_{\text{eff}}^{[n]})$ is a transition matrix that is a probability of exchanging configurations of the m th and n th replicas. Using the above equations,

$$\frac{T(\{R\}, W_{\text{eff}}^{[m]}|\{R'\}, W_{\text{eff}}^{[n]})}{T(\{R'\}, W_{\text{eff}}^{[m]}|\{R\}, W_{\text{eff}}^{[n]})} = e^{-\beta\Delta}, \quad (20)$$

where $\Delta = \Delta V_{\text{eff}}^{[m]} + \Delta V_{\text{eff}}^{[n]}$, with

$$\begin{aligned} \Delta V_{\text{eff}}^{[m]} &= V_{\text{eff}}^{[m]}(\{R'\}) - V_{\text{eff}}^{[m]}(\{R\}), \\ \Delta V_{\text{eff}}^{[n]} &= V_{\text{eff}}^{[n]}(\{R\}) - V_{\text{eff}}^{[n]}(\{R'\}). \end{aligned} \quad (21)$$

Here, an effective potential $V_{\text{eff}}(\{R\})$ is defined as follows:

$$V_{\text{eff}}(\{R\}) = \frac{1}{M} \sum_{s=0}^M \bar{V}(R^{(s)}) - \frac{\ln \Phi_T(R^{(0)})}{\beta} - \frac{\ln \Phi_T(R^{(M)})}{\beta}. \quad (22)$$

Therefore, the transition probability can be expressed by

$$T(\{R\}, W_{\text{eff}}^{[m]}|\{R'\}, W_{\text{eff}}^{[n]}) = \min\{1, e^{-\beta\Delta}\}. \quad (23)$$

Then, combining the above exchange move with our hybrid Monte Carlo introduces a new method, the replica exchange variational path integral hybrid Monte Carlo (EXVPIHMC). In EXVPIHMC calculations, HMC and exchange moves are selected stochastically with a given ratio. When the scaling parameter α is small enough, the fictitious system has a liquid-like melted structure. During the exchange moves among the replicas connecting the original system with the fictitious melted system, the system can efficiently be sampled in the configuration space of the cluster, avoiding possible trapping in a metastable state in the original system.

III. COMPUTATIONAL DETAILS

In the present study, the hydrogen molecules are modeled to be spherical particles interacting via Silvera and Goldman's potential.⁴⁹ The following trial wavefunction is adopted for all the clusters:

$$\Phi_T(R) = \prod_{i<j}^N \exp\left\{-\frac{1}{2}\left(\frac{b}{r_{ij}}\right)^5 - \frac{r_{ij}}{p}\right\}, \quad (24)$$

where b and p are variational parameters. The parameter $b = 3.70 \text{ \AA}$ is adopted for all the clusters, and the parameter p depends on the size of the cluster N : $p(N) = 2.24 + ((23.6 - 2.24)/47.0) \times (N - 3.0) \text{ \AA}$.⁹ These values have been obtained by optimizing the trial wavefunction of *para*-hydrogen clusters modeled by an isotropic pairwise interaction by Buck *et al.*⁵⁰ Suzuki and Chin type fourth order approximation with $\gamma = 0$ is adopted to approximate the short-time propagator; the superiority of this choice has been verified analytically for a harmonic oscillator and numerically for a realistic system in Ref. 32. The projection time $\beta = 1.2 \text{ K}^{-1}$ is used for all the variational path integral calculations. The imaginary time action is discretized with the number of time slices $M = 300$; the corresponding imaginary time increment is $\Delta\tau = \beta/M = 0.004 \text{ K}^{-1}$. These parameters have been tested in our previous study.³² In the present study, the variational path integral calculations have been performed using the staging

variables.^{45,46,51} The fictitious masses for the staging variables $m^{(s)}$ were set to be equal to the corresponding staging masses except end-point coordinates (at $s = 0$ and M) where $m^{(0)} = m^{(M)} = \gamma_{\text{ep}}m$; here, γ_{ep} is a parameter usually taken to be a positive number less than unity. In the present study, $\gamma_{\text{ep}} = 4/M$.

Variational path integral molecular dynamics calculations have been performed for the size of clusters, $N = 3, \dots, 40$. The time increment Δt was taken to be 9.0–12.0 fs to stably solve the equations of motion. Long molecular dynamics calculations have been performed to accurately evaluate various physical quantities such as kinetic and potential energies. While for $N = 3, \dots, 24$, we have performed 5×10^6 MD steps, for larger clusters $N \geq 25$, we needed to perform longer MD calculations ranging from 1×10^7 to 7×10^7 steps; for example, for $N = 26$, 2×10^7 MD steps with $\Delta t = 10$ fs corresponding to 200 ns.

In the replica exchange VPIHMC calculations, we have used $L = 11$ replicas; the scaling parameter of the intermolecular interaction for each replica is given to be $\alpha^{\ell} = 1.0 - 0.05 \times \ell$ for $\ell = 0, \dots, L - 1$. The exchange move is applied to the pair of adjacent replicas, ℓ and $\ell + 1$. In one MC step, we perform $L - 1$ exchange moves and one HMC move on average. The replica exchange VPIHMC calculations have been performed by 2×10^6 MC steps for the clusters of $N = 25, 26$, and 27. In one HMC step, 10 MD steps are performed with $\Delta t = 7$ fs.

IV. ENERGETICS AND STRUCTURAL FLUCTUATION IN THE CLUSTERS

We first show the total energy of the clusters by our variational path integral molecular dynamics (VPIMD) method. Two size regimes, $3 \leq N \leq 20$ and $21 \leq N \leq 40$, are separately presented in Tables I and II, respectively. Published data by the ground state quantum Monte Carlo (QMC) methods are collected in the tables. The diffusion Monte Carlo (DMC) results¹⁵ are presented for the size $3 \leq N \leq 40$. We find our VPIMD energies are in excellent agreement with DMC energies for the size $3 \leq N \leq 25$. For $N \geq 26$, VPIMD energies are consistent with DMC energies; however, a small discrepancy in the order of 0.1 K/molecule is found; the VPIMD energy of $N = 40$ is 0.4 K/molecule lower compared with the DMC energy, which is the largest discrepancy between VPIMD and DMC results. The observed discrepancy could arise from the bias due to the number of walkers N_w in DMC calculations. Statistically significant bias is reported for the cluster $N = 30$ in the addendum in Ref. 15, while no effect by N_w is found for smaller clusters $N = 10$ and 20; this observation is consistent with the trend in the discrepancy between VPIMD and DMC energies. Another source of discrepancy could be ascribed to the constraint imposed by the importance sampling function in DMC calculations. While the importance sampling function to describe liquid-like clusters is used in Ref. 15, another function to describe solid-like clusters is suggested to give a lower DMC energy for large clusters $N \geq 32$.¹⁹ The variational path integral is free from such constraint; one does not have to impose a solid symmetry in the trial wavefunction to get a solid.^{22,25}

TABLE I. Total energy of the clusters for size N , $3 \leq N \leq 20$, is listed in units of K/molecule. Two sets of the path integral ground state (PIGS) results^{8,16} are collected. DMC indicates the diffusion Monte Carlo results.⁹ DVR indicates the discrete variable representation result reported in Ref. 8. Statistical error in the last digit is indicated in parentheses.

N	Present work	PIGS ^a	PIGS ^b	DMC	DVR
3	-4.42(4)	-4.32(3)		-4.407(3)	-4.39
4	-6.90(4)	-6.76(2)		-6.898(3)	
5	-9.20(6)	-9.02(2)		-9.146(2)	
6	-11.14(5)	-10.92(2)		-11.145(2)	
7	-12.84(5)	-12.62(2)		-12.877(1)	
8	-14.49(6)	-14.11(2)		-14.428(1)	
9	-15.87(5)	-15.46(2)		-15.829(2)	
10	-17.18(5)	-16.72(2)		-17.141(3)	
11	-18.45(5)	-18.00(2)	-18.54(2)	-18.431(1)	
12	-19.75(5)	-19.24(2)	-19.77(2)	-19.713(3)	
13	-21.02(5)	-20.49(2)	-21.10(2)	-20.964(4)	
14	-21.96(5)	-21.20(1)	-22.00(2)	-21.902(3)	
15	-22.78(5)	-22.20(1)	-22.87(2)	-22.741(3)	
16	-23.53(4)	-22.95(1)	-23.65(2)	-23.488(4)	
17	-24.20(5)	-23.65(1)	-24.31(2)	-24.209(3)	
18	-24.91(4)	-24.34(1)	-25.05(2)	-24.902(3)	
19	-25.63(5)	-25.03(1)	-25.73(2)	-25.595(3)	
20	-26.29(4)	-25.69(1)	-26.40(2)	-26.268(4)	

^aReference 8.

^bReference 16.

In the tables, other ground state QMC results, the path integral ground state (PIGS) that is equivalent to the variational path integral, are also listed. Two sets of total energies by the PIGS method are presented. An earlier study⁸ covers

TABLE II. Total energy of the clusters for size N , $21 \leq N \leq 40$, is listed in units of K/molecule. The PIGS indicates the path integral ground state results.¹⁶ DMC indicates the diffusion Monte Carlo results.⁹ EXVPIHMC indicates the replica exchange variational path integral hybrid Monte Carlo results of the present study. Statistical error in the last digit is indicated in parentheses.

N	VPIMD	PIGS	DMC	EXVPIHMC
21	-26.94(4)	-27.08(2)	-26.901(5)	
22	-27.54(4)	-27.61(2)	-27.518(4)	
23	-28.18(4)	-28.27(2)	-28.113(3)	
24	-28.74(5)	-28.83(2)	-28.688(5)	
25	-29.30(3)	-29.41(2)	-29.241(4)	-29.25(6)
26	-29.92(2)	-29.96(2)	-29.772(3)	-29.88(9)
27	-30.38(3)	-30.51(2)	-30.272(5)	-30.28(6)
28	-30.83(3)	-30.94(2)	-30.739(2)	
29	-31.40(3)	-31.40(2)	-31.192(3)	
30	-31.73(3)	-31.83(2)	-31.635(7)	
31	-32.12(3)	-32.23(2)	-32.047(4)	
32	-32.59(2)	-32.63(2)	-32.439(8)	
33	-33.01(2)	-33.06(2)	-32.829(7)	
34	-33.66(2)	-33.68(2)	-33.188(9)	
35	-33.84(2)	-33.89(2)	-33.551(7)	
36	-34.09(2)	-34.20(2)	-33.898(6)	
37	-34.45(2)	-34.49(2)	-34.228(5)	
38	-34.78(2)	-34.82(2)	-34.532(6)	
39	-35.25(3)	-35.24(2)	-34.832(7)	
40	-35.53(1)	-35.55(2)	-35.136(7)	

the size regime $3 \leq N \leq 20$ and the later study¹⁶ extends the size regime $11 \leq N \leq 55$. In both studies, the same Monte Carlo algorithm was adopted to perform PIGS calculations with the Suzuki-Chin fourth order propagator. As found in the tables, our VPIMD energies are consistent with two sets of PIGS energies for all the cluster sizes presented. We first find a small discrepancy between PIGS results for $11 \leq N \leq 20$ in the energy range of 0.1–0.6 K/molecule. Since these two calculations have been performed using the same parameters β and $\Delta\tau$, the observed discrepancy could be attributed to the length of Monte Carlo run. Our VPIMD energies are in better agreement with the later PIGS results. VPIMD energies are, however, about 0.1 K/molecule higher compared with PIGS energies for the size $11 \leq N \leq 31$. For larger clusters, VPIMD energies are found to be in good agreement with PIGS energies (except $N = 36$). In Ref. 20, PIGS calculations using a Langevin equation (LE) have been reported for $4 \leq N \leq 19$ and $N = 33$. Total energies are found to be about 0.1 K/molecule smaller than the previous MC results,¹⁶ the small discrepancy is suggested to be due to the slightly different $\Delta\tau$ values, $\Delta\tau = 0.003 \text{ K}^{-1}$ for LE and 0.0015625 K^{-1} for MC. Since $\Delta\tau = 0.004 \text{ K}^{-1}$ is demonstrated to be small enough for the cluster of $N = 20$,³¹ the small discrepancy between MC and LE results could be due to the run length; the LE calculations are reported to be performed in 5 ns, while the MC run length is not reported in the Ref. 8 though. As described in Sec. III, we have found quite long molecular dynamics calculations are needed to properly evaluate the statistical error of the kinetic and potential energies; we have performed molecular dynamics calculations ranging from 50 ns to 630 ns for broadly sampling the potential energy landscape of the clusters.

We next examine the stability of the *para*-hydrogen clusters based on the classical approximation. This is carried out by minimizing the potential energy of the clusters by the steepest descent method; an initial configuration for each cluster minimization was taken from the global minimum structure database for the corresponding Lennard-Jones cluster.⁵² To precisely discuss the stability of the clusters, we introduce the “classical chemical potential” of the cluster of the size N defined by $\mu_N = (V_{\text{mim}})_N - (V_{\text{mim}})_{N-1}$, where $(V_{\text{mim}})_N$ is the minimum potential energy of the cluster of the size N . The size dependence of the classical μ_N is presented in Fig. 1. As seen in the figure, the classical chemical potential shows rich size dependence; minima in the size dependence are found for $N = 7, 13, 19, 23, 26, 29, 32, 34, 36$, and 39 . Within the classical approximation, these clusters can be regarded to be stable compared with their neighboring size clusters. We next show the quantum chemical potential defined by $\mu_N = \langle H \rangle_N - \langle H \rangle_{N-1}$, where $\langle H \rangle_N$ is the total energy of the cluster of the size N . The size dependence is presented in Fig. 2. Many minima found in the classical μ_N are diminished; the survived minima are found for $N = 13, 26, 29, 34$, and 39 . Here and hereafter, these stable clusters are referred to be magic number clusters. In Fig. 2, we also show the chemical potentials calculated by other quantum Monte Carlo methods; diffusion Monte Carlo (DMC),¹⁵ path integral ground state (PIGS),¹⁶ and path integral Monte Carlo (PIMC);¹¹ the PIMC results for clusters at temperature 0.5 K. Up to $N \approx 25$, our VPIMD results are found to be in

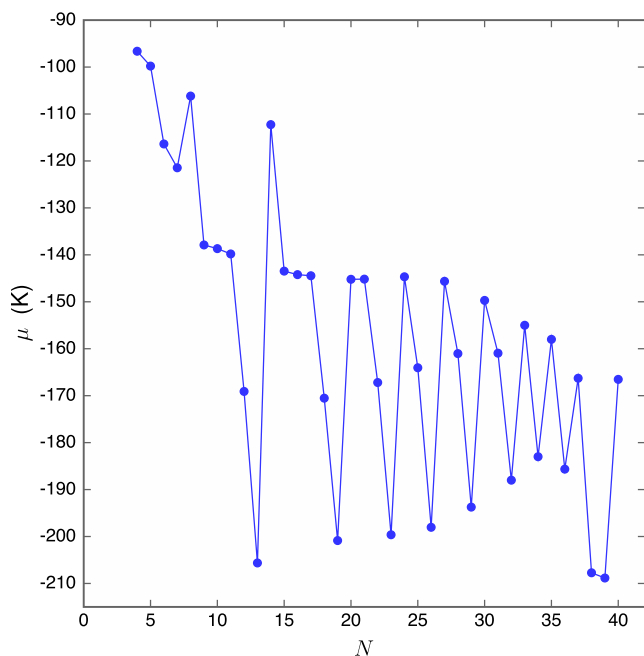


FIG. 1. Classical chemical potential μ_N is shown as a function of the cluster size N . Filled blue circles indicate the chemical potential and the line is drawn as an aid to the eye.

good agreement with the DMC, PIGS, and PIMC results. For larger clusters, our VPIMD results agree well with the PIMC results. In the range of the size, $26 \leq N \leq 32$, the amplitude of the oscillation in the size dependence is systematically smaller than the PIMC results. This could be ascribed to the quantum enhancement of the fluctuation in the clusters with

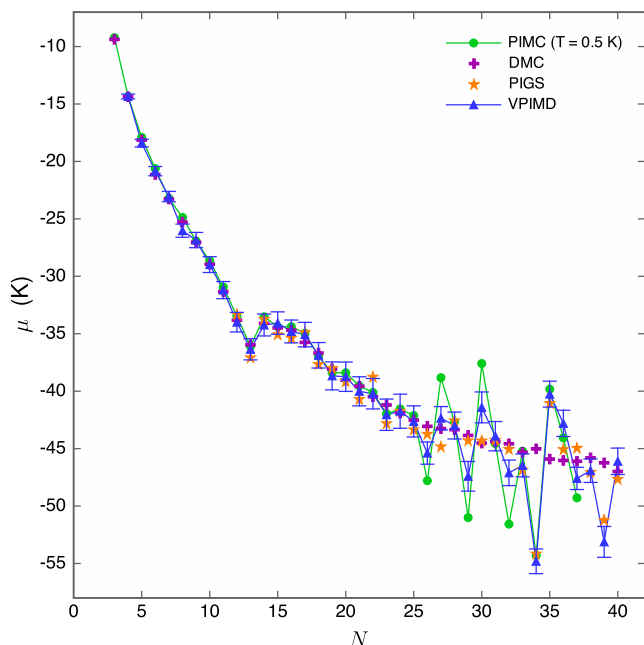


FIG. 2. Quantum chemical potential μ_N is shown as a function of the cluster size N . Blue triangles are the variational path integral molecular dynamics results. Green circles are the path integral Monte Carlo results for clusters at $T = 0.5$ K,¹¹ purple cross symbols are the diffusion Monte Carlo results¹⁵ and orange star symbols are the path integral ground state results.¹⁶ The line is drawn as an aid to the eye.

lowering temperature.^{11,17} On the other hand, DMC results show monotonic size dependence even for $N \geq 25$. In Ref. 15, the zigzag size dependence found in the PIMC results is suggested to be a finite temperature effect. However, our VPIMD results clearly show that the size dependence exists even in the ground state. PIGS results are found to be in good agreement with VPIMD results for the size $N \geq 33$, showing the zigzag size dependence in the ground state. In the size regime $26 \leq N \leq 32$, however, PIGS results are less structured than VPIMD results. This arises from the small discrepancy in total energies between VPIMD and PIGS calculations for the size regime, which could be due to the length of run as discussed above.

To understand the size dependence more deeply, we decompose the chemical potential into the kinetic and potential energy contributions: $\mu_N = \Delta\langle T \rangle_N + \Delta\langle V \rangle_N$, where $\Delta\langle O \rangle_N = \langle O \rangle_N - \langle O \rangle_{N-1}$ for an operator O . The size dependence of these contributions is shown in Fig. 3. Deep minima in the potential energy contribution are found for $N = 13, 26, 29, 34$, and 39 . Although the corresponding kinetic energy contributions have maxima for the clusters, the potential energy contribution outperforms the kinetic energy contribution. Shallow minima in the potential energy contribution, $N = 23, 32$, and 37 are almost washed out by the kinetic energy contribution.

We next discuss the stability from the structural viewpoint. Density profile measured from the center of mass is shown for $N = 25, 26$, and 27 in Fig. 4. The cluster of $N = 26$ shows the magic number stability found in the chemical potential. All the clusters presented in the figure have structured density profiles. As is evident from the figure, the density profile for

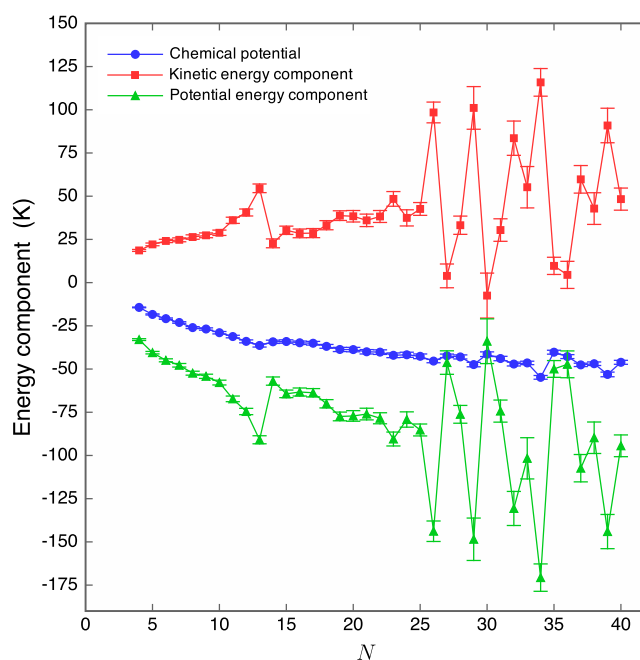


FIG. 3. Quantum chemical potential μ_N and the kinetic and potential energy components of μ_N are shown as a function of the cluster size N . Blue circles, red squares, and blue triangles are the quantum chemical potential, kinetic energy component, and potential energy component, respectively. The line is drawn as an aid to the eye.

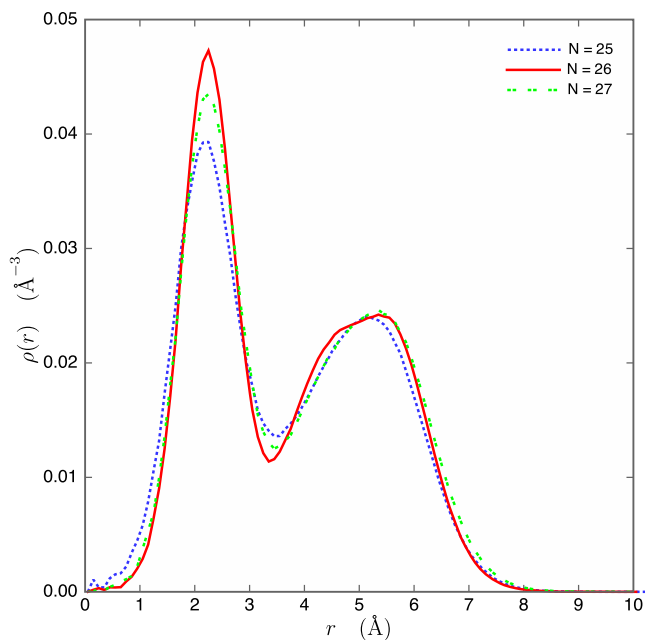


FIG. 4. Radial density profile measured from the center of the cluster $\rho(r)$ is shown. Dotted blue, solid red, and dashed green curves are the results for the size $N = 25, 26,$ and $27,$ respectively.

$N = 26$ is found to be more rigid compared with the neighboring size clusters $N = 25$ and 27 . This structural rigidity yields the magic number stability. Other magic number clusters $N = 29$ and 34 show the same structural trend. In Fig. 5, the density profile is shown for $N = 38, 39,$ and 40 . It seems that the cluster is undergoing a structural change with approaching $N = 40$, suggesting a different physical origin in the magic number stability. This point will be addressed in a future study.

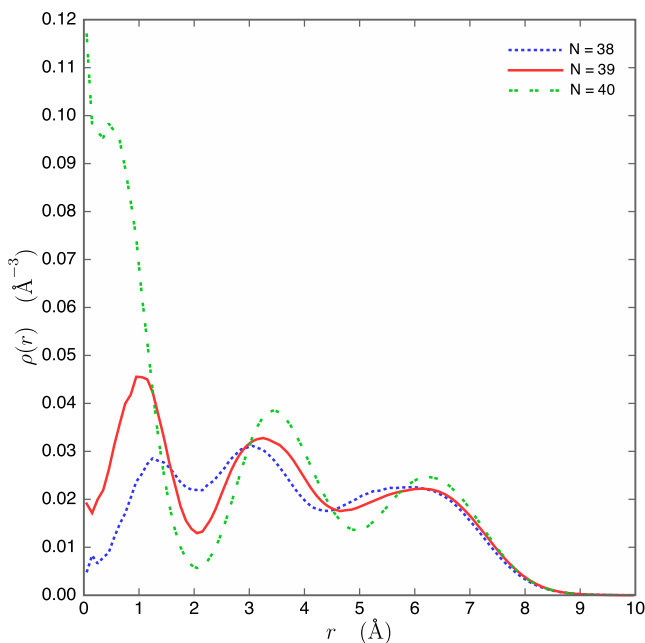


FIG. 5. Radial density profile measured from the center of the cluster $\rho(r)$ is shown. Dotted blue, solid red, and dashed green curves are the results for the size $N = 38, 39,$ and $40,$ respectively.

V. HIDDEN STRUCTURES

In this section, we apply the inherent structure analysis to our VPIMD method to characterize the wavefunction of the clusters in the configuration space. The inherent structure analysis has originally been developed to classical systems at finite temperatures;⁵³ configurations generated by molecular simulation methods are numerically minimized along the trajectory. The procedure corresponds to instantaneously quench the system at absolute zero, revealing the potential energy landscape explored by the kinetic energy of the system. The method

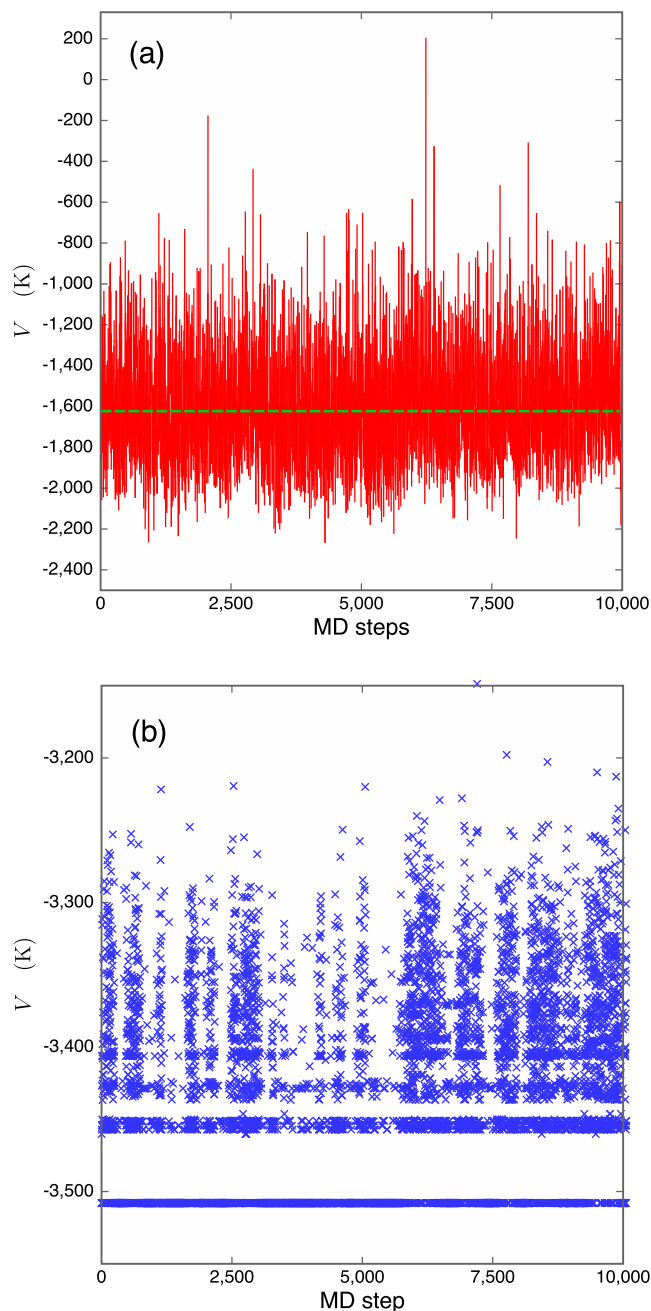


FIG. 6. (a) The instantaneous potential energy of the cluster of $N = 26$ at the imaginary time $\tau = \beta/2$ is shown along the variational path integral molecular dynamics (VPIMD) trajectory. The dashed line indicates the expected value of the potential energy. (b) The potential energy of the corresponding inherent structures is shown along the VPIMD trajectory. The potential energy for the global minimum structure is given to be -3507.9 K.

has been extended to quantum systems studied by DMC and PIMC.⁵⁴ In the present study, we have applied the idea of the inherent structures to the VPIMD results. As described in Sec. II, the structures at the imaginary time $\tau = \beta/2$ are distributed according to the square of the exact wavefunction $|\Psi_0|^2$. Then, each structure along the VPIMD trajectory is minimized by the steepest descent method.

In Fig. 6, we show the potential energy of the cluster of $N = 26$ along the VPIMD trajectory. The potential energy is calculated at the imaginary time slice $\tau = \beta/2$. The instantaneous energy fluctuates around an averaged value. In the figure, the potential energy of the inherent structures is also presented. A band in the lowest energy is found to be the energy of the global minimum structure. As is evident from the figure, the wavefunction is highly delocalized in the configuration space; the wavefunction covers high energy local minima as well as the global minimum. We confirmed that wavefunctions for clusters $N = 25$ and 27 are also delocalized in the configuration space. In Fig. 7, the energy gap between the global minimum and the second lowest minimum is shown as a function of the cluster size N . We find the energy gap of $N = 26$ is larger compared with that for $N = 25$ and 27 , which means that the global minimum energy structure of the magic number cluster is stabler than that of the neighboring size clusters. This stability of the global minimum causes the magic number stability observed in the chemical potential. Other magic number clusters $N = 29$ and 34 show the same trend of the stability of the global minimum structure.

In Fig. 8, the potential energy difference $\Delta\langle V \rangle$ calculated using the inherent structures is presented. The size dependence observed in $\Delta\langle V \rangle$ is found to be well described by the inherent structures, indicating that the zigzag dependence of the chemical potential reflects the potential energy landscape of each cluster.

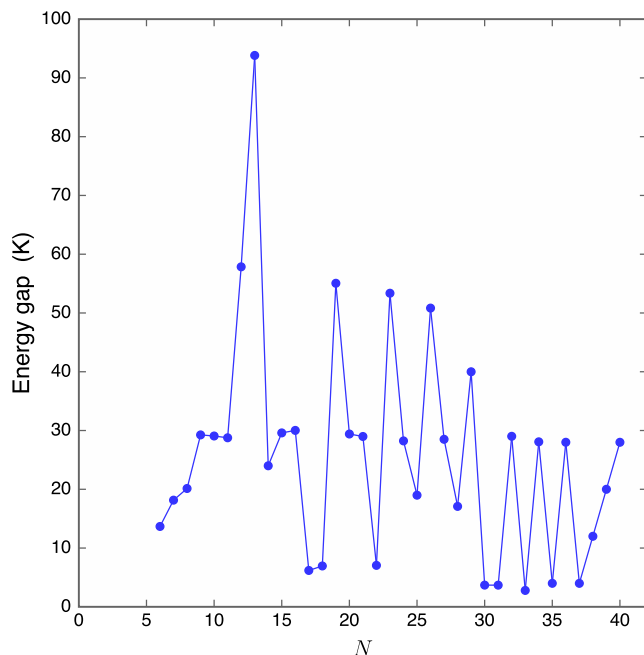


FIG. 7. Energy gap between the global minimum energy and the second lowest energy minimum is shown as a function of the cluster size N . The line is drawn as an aid to the eye.

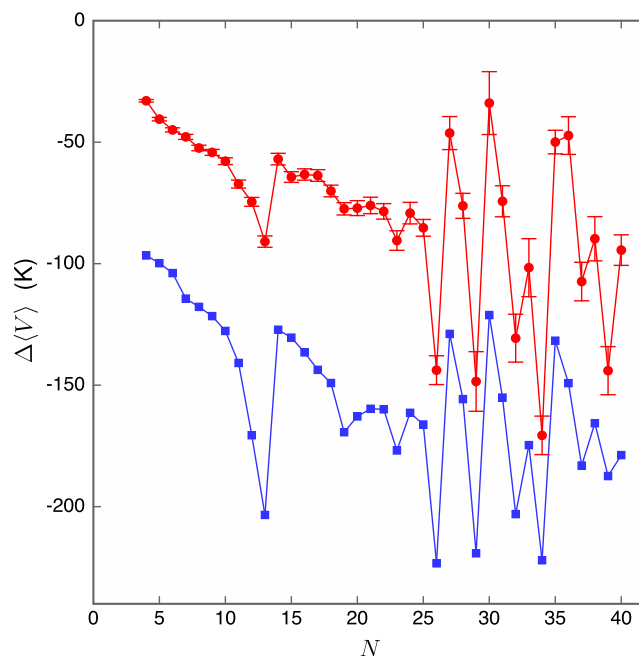


FIG. 8. Potential energy component of μ_N is shown as a function of the cluster size N . Blue squares are the results by the inherent structure analysis. The $\Delta\langle V \rangle$ of the quantum μ_N is also presented for comparison (red circles). The line is drawn as an aid to the eye.

VI. QUEST FOR THE TRUE GROUND STATE

In this section, we present the ground state properties of *para*-hydrogen clusters $N = 25, 26$, and 27 by our replica exchange path integral hybrid Monte Carlo (EXVPIHMC) method. This provides a stringent test on the reliability of our molecular dynamics results presented in Secs. IV and V. For EXVPIHMC calculations, we have prepared replicas covering from structured to fully melted clusters to minimize the possibility on trapping in metastable states. To realize this, we adopted scaling parameter α of the potential energy in the range $0.5 \leq \alpha \leq 1.0$; as demonstrated below, the interaction with $\alpha = 0.5$ corresponds to a fully melted system.

We first optimize the variational parameters of the trial wavefunctions for each replica; the same functional form Eq. (24) is used for all the replicas. Scaling parameter for an ℓ th replica is given by $\alpha^{|\ell|} = 1.0 - 0.05 \times \ell$ for $\ell = 0, \dots, 10$. Numerical optimization of the variational parameters has been performed by our variational molecular dynamics (VMD) method²⁴ combined with the steepest descent minimization. The VMD is a method compatible with the variational Monte Carlo method, which is used to numerically evaluate the derivatives of the total energy regarding the variational parameters. In Fig. 9, a density profile by the optimized trial wavefunction is presented for $N = 26$. The cluster with $\alpha = 1.0$ shows a two-peak structured profile. With decreasing α , the density profile becomes broader; the cluster is fully melted for $\alpha = 0.5$. Using the trial wavefunctions, we have performed the replica exchange VPIHMC calculations. For each pair of replicas, the acceptance ratio of the exchange trials was found to be about 10%. In Fig. 10, the exchange diagram is presented. This diagram indicates how a cluster starting from a replica travels other replicas by the exchange MC move along the EXVPIHMC trajectory. As is evident from the figure, the

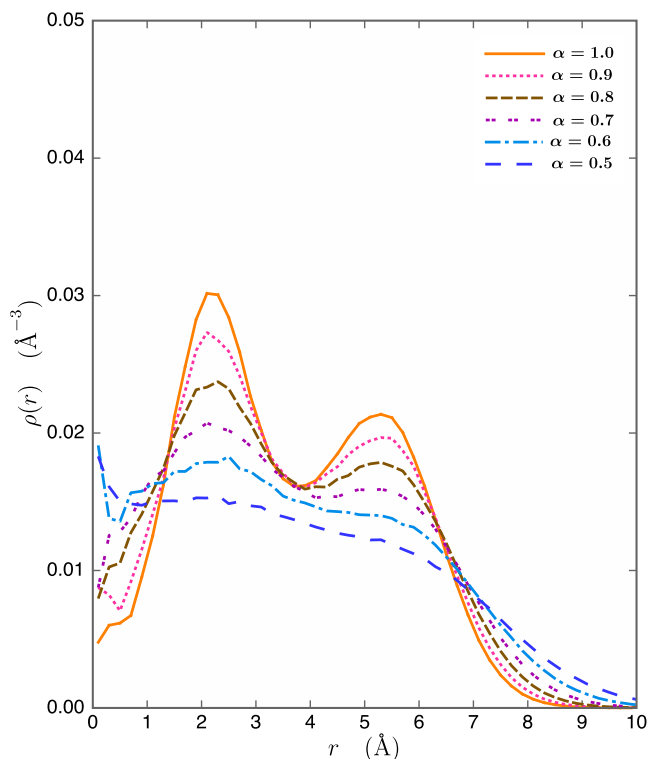


FIG. 9. Radial density profile measured from the center of the cluster $\rho(r)$ is shown for $N = 26$. The density profile is calculated using the optimized trial wavefunction for the system with the scaling parameter of the intermolecular interaction, $\alpha = 1.0$ (solid), 0.9 (dotted), 0.8 (dashed), 0.7 (twisted), 0.6 (chain), and 0.5 (sparse).

cluster starting from a replica widely wanders all the replicas ranging from the structured to the fully melted clusters. This indicates that a system could escape from a metastable state

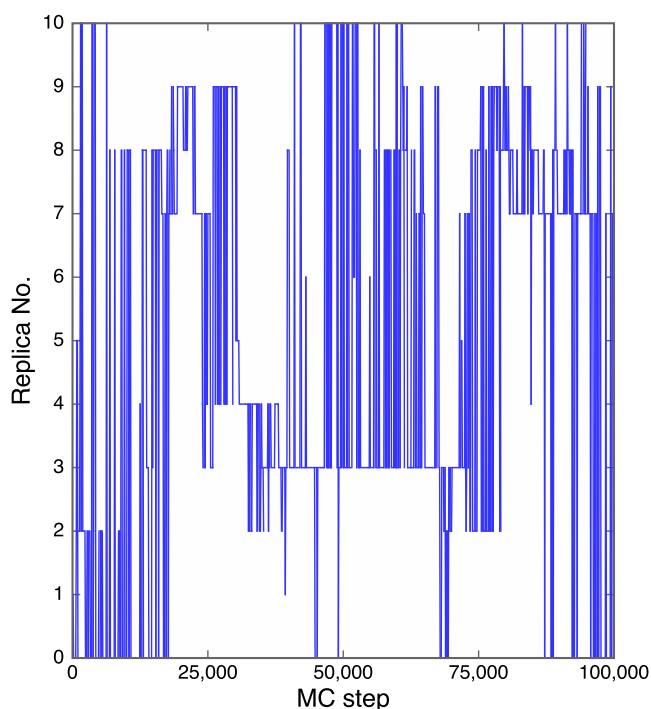


FIG. 10. Replica number occupied by the cluster starting from a replica is shown along the replica exchange variational path integral hybrid Monte Carlo step.

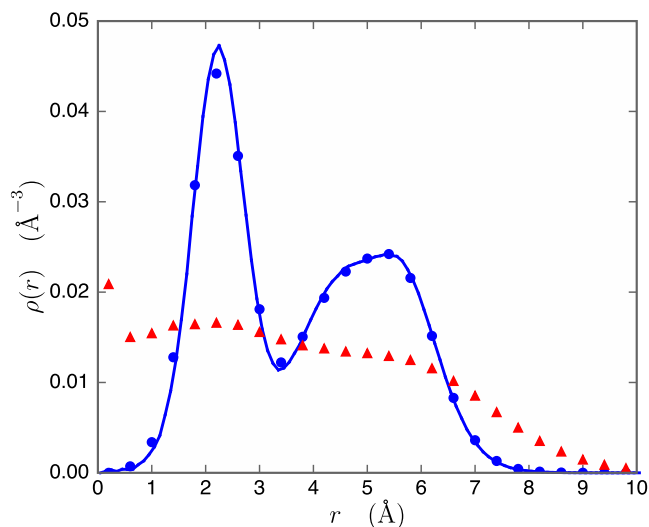


FIG. 11. Radial density profile measured from the center of the cluster is shown for $N = 26$. Blue circles are the results by the replica exchange variational hybrid Monte Carlo method with $\alpha = 1.0$ and red triangles with $\alpha = 0.5$. Solid curve is given by the variational path integral molecular dynamics results.

via the exchange moves even if the system would be stuck in the metastable state. Figure 11 shows the density profiles of the cluster of $N = 26$ for two scaling parameters $\alpha = 1.0$ and 0.5. While the cluster with the scaling parameter $\alpha = 1.0$ has the structured profile, the cluster with $\alpha = 0.5$ is found to be melted in the ground state. This demonstrates that the ground state of the *para*-hydrogen cluster modeled by Silvela and Goldman's potential is not described by the melted profile but by the structured density profile. Other clusters $N = 25$ and 27 are found to show the same structural trend. In Table I, the total energies are collected for $N = 25$, 26, and 27 clusters calculated by EXVPIHMC and VPIMD. The results are in good agreement, indicating the reliability of our VPIMD results.

VII. CONCLUDING REMARKS

In the present study, ground state properties of *para*-hydrogen clusters up to the size of $N = 40$ have been studied by the variational path integral method. Our variational path integral molecular dynamics calculations have revealed that the *para*-hydrogen clusters indicate the magic number stability for the sizes $N = 13, 26, 29, 34$, and 39, which is manifested in minima in the size dependence of the chemical potential of the hydrogen molecule. The zigzag size dependence of the chemical potential found in the finite temperature path integral Monte Carlo study¹¹ exists even at zero temperatures. The magic number clusters were found to have a larger structural rigidity compared with the neighboring size clusters. The inherent structure analysis, which has been extended to the variational path integral, reveals the magic number stability well described by the potential energy landscape of the clusters, especially the stability of the global minimum energy structure.

We have also developed a novel simulation method combining our variational path integral hybrid Monte Carlo method with the replica exchange technique. In the present study, we scale the potential energy of the cluster to introduce

replicas whose structures cover from rigid to melted systems. Our replica exchange variational path integral hybrid Monte Carlo method has been applied to selected clusters $N = 25$, 26, and 27. The calculated results demonstrate the reliability of our variational path integral molecular dynamics results, indicating the *para*-hydrogen clusters have the structured density profile in the ground state.

It is important to directly address the issue of the superfluidity of the *para*-hydrogen clusters to connect our findings in the present study with the superfluidity. We need to develop a method to evaluate the superfluid density of free clusters within the variational path integral framework. Associated with this issue, the off-diagonal component of the density matrix must be calculated to directly evaluate the condensate fraction. This can be realized by extending our VPIMD method to the off-diagonal density matrix. These issues will be addressed in the future.

- ¹V. L. Ginzburg and A. A. Sobyenin, *JETP Lett.* **15**, 242 (1972).
- ²O. N. Osychenko, R. Rota, and J. Boronat, *Phys. Rev. B* **85**, 224513 (2012).
- ³G. Tejeda, J. M. Fernández, S. Montero, B. Blume, and J. P. Toennies, *Phys. Rev. Lett.* **92**, 223401 (2004).
- ⁴K. Kuyanov-Prozumnet and A. F. Vilesov, *Phys. Rev. Lett.* **101**, 205301 (2008).
- ⁵J. P. Toennies and A. F. Vilesov, *Angew. Chem., Int. Ed.* **43**, 2622 (2004).
- ⁶P. Sindzingre, D. M. Ceperley, and M. L. Klein, *Phys. Rev. Lett.* **67**, 1871 (1991).
- ⁷F. Mezzacapo and M. Boninsegni, *Phys. Rev. Lett.* **97**, 045301 (2006).
- ⁸J. E. Cuervo and P.-N. Roy, *J. Chem. Phys.* **125**, 124314 (2006).
- ⁹R. Guardiola and J. Navarro, *Phys. Rev. A* **74**, 025201 (2006).
- ¹⁰E. Rabani and J. Jortner, *J. Phys. Chem. B* **110**, 18893 (2006).
- ¹¹S. A. Khairallah, M. B. Sevryuk, D. M. Ceperley, and J. P. Toennies, *Phys. Rev. Lett.* **98**, 183401 (2007).
- ¹²F. Mezzacapo and M. Boninsegni, *Phys. Rev. A* **75**, 033201 (2007).
- ¹³F. Mezzacapo and M. Boninsegni, *Phys. Rev. A* **76**, 021201(R) (2007).
- ¹⁴F. Mezzacapo and M. Boninsegni, *Phys. Rev. Lett.* **100**, 145301 (2008).
- ¹⁵R. Guardiola and J. Navarro, *Cent. Eur. J. Phys.* **6**, 33 (2008).
- ¹⁶J. E. Cuervo and P.-N. Roy, *J. Chem. Phys.* **128**, 224509 (2008).
- ¹⁷M. B. Sevryuk, J. P. Toennies, and D. M. Ceperley, *J. Chem. Phys.* **113**, 064505 (2010).
- ¹⁸S. Warnecke, M. B. Sevryuk, D. M. Ceperley, J. P. Toennies, R. Guardiola, and J. Navarro, *Eur. Phys. J. D* **56**, 353 (2010).
- ¹⁹E. Sola and J. Boronat, *J. Phys. Chem. A* **115**, 7071 (2011).
- ²⁰M. Schmidt, S. Constable, C. Ing, and P.-N. Roy, *J. Chem. Phys.* **140**, 234101 (2014).
- ²¹J. D. Mallory and V. A. Mandelshtam, *J. Phys. Chem. A* **121**, 6341 (2017).
- ²²D. M. Ceperley, *Rev. Mod. Phys.* **67**, 279 (1995).
- ²³A. Sarsa, K. E. Schmidt, and W. R. Magro, *J. Chem. Phys.* **113**, 1366 (2000).
- ²⁴S. Miura, *Chem. Phys. Lett.* **482**, 165 (2009).
- ²⁵S. Miura, *Comput. Phys. Commun.* **182**, 274 (2011).
- ²⁶S. Miura, *Mol. Simul.* **38**, 378 (2012).
- ²⁷S. Miura, *J. Phys.: Conf. Ser.* **454**, 012023 (2013).
- ²⁸S. Miura, *GAKUTO Int. Ser., Math. Sci. Appl.* **34**, 129 (2011).
- ²⁹S. Miura, in *Quantum Systems in Chemistry and Physics*, edited by K. Nishikawa, J. Marauni, E. J. Brandas, G. Delgado-Barrio, and P. Piecuch (Springer, Dordrecht, 2012).
- ³⁰S. Miura, in *Advances in Quantum Monte Carlo*, ACS Symposium Series 1094, edited by S. Tanaka, S. M. Rothstein, and W. A. Lester, Jr. (American Chemical Society, Washington, DC, 2012).
- ³¹Y. Kamibayashi and S. Miura, *Mol. Simul.* **41**, 808 (2015).
- ³²Y. Kamibayashi and S. Miura, *J. Chem. Phys.* **145**, 074114 (2016).
- ³³K. Hukushima and K. Nemoto, *J. Phys. Soc. Jpn.* **65**, 1604 (1996).
- ³⁴E. Marinari, G. Parisi, and J. J. Ruiz-Lorenzo, in *Spin Glasses and Random Fields*, edited by A. P. Young (World Scientific, New Jersey, 1998).
- ³⁵W. M. C. Foulkes, L. Mitas, R. J. Needs, and G. Rajagopal, *Rev. Mod. Phys.* **73**, 33 (2001).
- ³⁶R. P. Feynman and A. R. Hibbs, *Quantum Mechanics and Path Integrals* (McGraw-Hill, New York, 1965).
- ³⁷R. P. Feynman, *Statistical Mechanics* (Addison-Wesley, Redwood City, 1972).
- ³⁸D. Chandler and P. G. Wolynes, *J. Chem. Phys.* **74**, 4078 (1981).
- ³⁹M. E. Tuckerman, *Statistical Mechanics: Theory and Molecular Simulation* (Oxford University Press, New York, 2010).
- ⁴⁰M. Suzuki, *Phys. Lett. A* **201**, 425 (1995).
- ⁴¹S. A. Chin, *Phys. Lett. A* **226**, 344 (1997).
- ⁴²S. Jang, S. Jang, and G. A. J. Voth, *J. Chem. Phys.* **115**, 7832 (2001).
- ⁴³T. Kashiwa, Y. Ohnuki, and M. Suzuki, *Path Integral Methods* (Oxford University Press, Oxford, 1997).
- ⁴⁴G. J. Martyna, M. L. Klein, and M. E. Tuckerman, *J. Chem. Phys.* **99**, 2796 (1993).
- ⁴⁵M. Tuckerman, B. J. Berne, G. J. Martyna, and M. L. Klein, *J. Chem. Phys.* **99**, 2796 (1993).
- ⁴⁶M. E. Tuckerman and A. Hughes, in *Classical and Quantum Dynamics in Condensed Phase Simulations*, edited by B. J. Berne, G. Cicciotti, and D. F. Coker (World Scientific, Singapore, 1999).
- ⁴⁷S. Duane, A. D. Kennedy, B. J. Pendleton, and D. Roweth, *Phys. Lett. B* **195**, 216 (1987).
- ⁴⁸B. Mehlig, D. W. Heermann, and B. M. Forrest, *Phys. Rev. B* **45**, 679 (1992).
- ⁴⁹I. F. Silvera and V. V. Goldman, *J. Chem. Phys.* **69**, 4209 (1978).
- ⁵⁰U. Buck, F. Huisken, A. Kohlhasse, D. Otten, and J. Schaeffer, *J. Chem. Phys.* **78**, 4439 (1983).
- ⁵¹S. Miura and J. Tanaka, *J. Chem. Phys.* **120**, 2160 (2004).
- ⁵²D. J. Wales, J. P. K. Doye, A. Dullweber, M. P. Hodges, F. Y. Naumkin, F. Calvo, J. Hernández-Rojas, and T. F. Middleton, The Cambridge Cluster Database, <http://www-wales.ch.cam.ac.uk/CCD.html>.
- ⁵³F. H. Stillinger and T. A. Weber, *Phys. Rev. A* **25**, 978 (1982).
- ⁵⁴F. H. Stillinger, *J. Chem. Phys.* **89**, 4180 (1988).